Criticality and marginal stability of the shear jamming transition of frictionless soft spheres

Varghese Babu[*] and Srikanth Sastry [†]

Theoretical Sciences Unit and School of Advanced Materials, Jawaharlal Nehru Center for Advanced Scientific Research, Jakkur Campus, Bengaluru 560064, India

We study numerically the critical behavior and marginal stability of the shear jamming transition for frictionless soft spheres, observed to occur over a finite range of densities, associated with isotropic jamming for densities above the minimum jamming (J-point) density. Several quantities are shown to scale near the shear jamming point in the same way as the isotropic jamming point. We compute the exponents associated with the small force distribution and the interparticle gap distribution and show that the corresponding exponents are consistent with the marginal stability condition observed for isotropic jamming and with predictions of the mean-field theory of jamming in hard spheres.

Jamming is a ubiquitous phenomenon, observed in a variety of physical systems classified as *granular matter* (sand, grains, powders), foams, colloids, etc., wherein thermal motion does not play a significant role. The jamming transition is typically observed when disordered materials are compressed, resulting in a transition to a state which can resist deformation [1]. Athermal frictionless soft spheres have served as an idealized model for studying the jamming transition [2–4] along with packings of hard spheres.

The jamming density ϕ_J has many properties of a critical point. The configurations at ϕ_J are isostatic with average coordination number $z = 2d = z_{\mathrm{iso}}$, where d is the spatial dimension [2–4]. As the system is compressed above the jamming density (for soft spheres) the excess coordination number $\delta z = z - z_{\mathrm{iso}}$ scales as $\delta z \sim (\phi - \phi_J)^{1/2}$, independent of the interaction potential and the configurations are mechanically stable [2–4]. The pressure vanishes linearly with $(\phi - \phi_J)$ with a prefactor depending on the interaction potential [2,4,5]. Close to, and above, the jamming density, the vibrational density of states (VDOS) $D(\omega)$, where ω is the frequency, displays anomalous behavior with the presence of excess low-frequency modes compared to the Debye solid which describe a normal elastic medium with a characteristic frequency ω^* vanishing as the jamming point is approached with a power-law dependence on $(\phi - \phi_J)$ [6–8]. Such aspects of critical-like behavior near the jamming point has been widely investigated and established [4,9].

The requirement of mechanical stability of jammed packings has been shown to imply an inequality or bound between exponents that characterize the distribution of interparticle forces f, which exhibits a power-law form $P_e(f) \sim f^{\theta_e}$ at small forces, and the distribution of distances or gaps h between particles that are nearly in contact, which exhibits a well known power-law singularity, $g(h) \sim h^{-\gamma}$ [10,11]. The bound $\gamma \geqslant 1/(2 + \theta_e)$ was argued to be saturated at jamming [10]

and that such a *marginal stability condition* provided a mechanism to explain the avalanches of rearrangement observed [12,13].

The mean-field theory of glass transition in hard spheres in the limit of infinite dimensions [14,15], interestingly, leads to predictions concerning the behavior at jamming, and, in particular, a prediction for the exponents θ_e and γ to be $\theta_e = 0.423\,11\cdots$ and $\gamma = 0.412\,69\cdots$. Whereas the predicted value of γ is close to those observed in two (2D), three dimensional (3D) packings, as well as higher dimensions [16], leading to the possibility that $d = 2$ constitutes the upper critical dimensions for the jamming transition, the reported values of exponent θ [11,16,17] exhibits a wide range. However, as noted in Ref. [11], the presence of localized excitations in finite dimensions leads to a modified distribution $P_l(f) \sim f^{\theta_l}$ and marginal stability condition $\gamma \geqslant (1 - \theta_l)/2$. The localized excitations were associated with sphere arrangements prone to buckling or *bucklers* in Ref. [18], and separating out the distributions of forces corresponding to bucklers leads to the verification of marginal stability condition with the exponents predicted by mean-field theory.

In this Letter, we examine the validity of these aspects of criticality and marginal stability for the shear jamming transition for frictionless soft spheres in two and three dimensions and show that they are indeed valid. The jamming of granular matter under shear has been observed experimentally [19,20] and numerically [21–23] for frictional systems. However, friction is not necessary for the shear jamming transition [24–30]. In Ref. [26], critical behavior near the shear jamming transition for frictionless soft spheres were considered in 3D. Although the density range over which shear jamming occurs was seen to vanish in the thermodynamic limit, the behavior of the pressure, contact number z, and the bulk modulus were shown to exhibit the same behavior as a function of shear stress (equivalently, shear strain above the jamming strain) as at the isotropic jamming point. The key difference is that both the bulk modulus B and the shear modulus G remain finite at the shear jamming point, unlike the isotropic case where only the bulk modulus is finite. Nevertheless, only a single
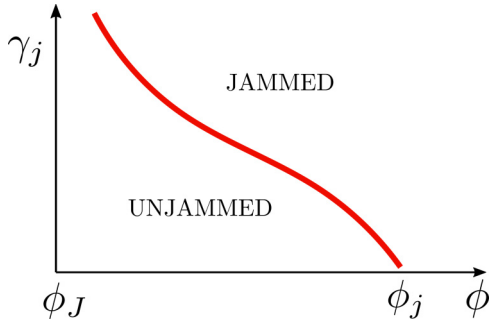
_____
[*]varghese@jncasr.ac.in
[†]sastry@jncasr.ac.in

FIG. 1. Schematic showing the existence of shear jamming for configurations above the minimum jamming density ϕ_J.

eigenvalue of the elastic modulus tensor becomes finite, and the finite values of B and G can be understood in terms of a rotation of the eigenvectors, leading to the conclusion that shear jamming and the isotropic case have the same symmetry and critical behavior. Similar conclusions have been arrived at in other investigations [28,31].

However, shear jamming can occur over a finite range of densities even in the absence of friction [24,25,27,28]. This is related to the presence of a range of densities (J line) over which isotropic jamming can take place, above the minimum jamming density ϕ_J (of ≈ 0.648 for $d = 3$ and ≈ 0.84 for $d = 2$). When the preparation history dependent jamming density of a packing ϕ_j is $> \phi_J$, decompression of the packing to densities ϕ, $\phi_J < \phi < \phi_j$ leads to unjamming, but such unjammed packings can jam under the application of shear [27,28] as shown in Fig. 1 (the jamming density $\phi_j \approx \phi_J$ in Ref. [26], and, hence, the finite shear jamming range is not observed). It is, therefore, of interest to investigate the critical behavior of shear jamming over such density intervals, which we do, building on previous work [23,26,28,29]. With the distance from the shear jamming strain $\gamma - \gamma_j$ playing the role of the excess density above jamming, $\phi - \phi_j$ for isotropic jamming, we find that the scaling of pressure, excess contact number, shear stress, and the behavior of the VDOS $D(\omega)$ is the same as at isotropic jamming. In addition, we explore in detail the marginal stability condition, employing the approach of Ref. [18] to distinguish localized excitations or *bucklers* and demonstrate that the behavior for shear jamming is consistent with that for isotropic jamming and mean-field predictions. Other than a preliminary investigation in Ref. [22], the applicability of the marginal stability condition for shear jamming has not been investigated. Our results, thus, clearly demonstrate that properties related to criticality and marginal stability for shear jamming are the same as for isotropic jamming.

Model and methods: The systems we study are bidisperse soft sphere mixtures (50:50) in 2D and 3D with a harmonic repulsive interparticle potential. The interaction potential is given by $v(|\vec{r}_{ij}|) = \epsilon(1 - \frac{|\vec{r}_{ij}|}{\sigma_{ij}})^2$ for $|\vec{r}_{ij}| \leqslant \sigma_{ij}$ where $\vec{r}_{ij}$ is the vector connecting the centers of particles i and j and $\sigma_{ij} = \frac{\sigma_i + \sigma_j}{2}$ with σ_k being the diameter of particle type $k(\sigma_2/\sigma_1 = 1.4)$. The first step in our Letter involves generating configurations with jamming density $\phi_j > \phi_J$. For this we follow the protocol similar to the one used in Ref. [5] which we describe

for $d = 3$ briefly; other procedures that could be employed are outlined in Refs. [27,32]. At the packing fraction $\phi = 0.5935$ we generate configurations by initializing particle centers randomly and performing an energy minimization to generate configurations with no overlaps (a configuration with no overlap is considered unjammed). This configuration is treated as a configuration of hard spheres and equilibrated by hard-sphere Monte Carlo simulation using HOOMD [33,34]. We then compress the system in steps of $\delta\phi = 10^{-4}$, performing an energy minimization after each compression. Compression is carried out by changing the box dimensions of the system. When the jamming density ϕ_j is crossed, the energy after minimization e/N will be greater than 10^{-24}. When the energy crosses a threshold (here $\frac{e}{N} > 10^{-7}$) we stop the compression and start decompressing the system with smaller steps of $\delta\phi = 10^{-5}$. During the decompression when we are able to minimize the energy to $\frac{e}{N} < 10^{-24}$ we stop the process and identify the jamming density. The jamming densities obtained through the procedure are distributed around $\phi \approx 0.661$, which depends on the density of the initial equilibrated fluid [5]. From the configurations at ϕ_j we generate unjammed configurations at $\phi_J < \phi < \phi_j$ by scaling the volume.

These configurations are sheared uniformly using athermal quasistatic (AQS) shear to observe shear jamming at a strain γ_j, employing the Large-scale Atomic/Molecular Massively Parallel Simulator [35]. AQS shear for a strain step $\delta\gamma$ is carried out by performing an affine transformation $x_i \to x_i + \delta\gamma y_i$; $y_i \to y_i$; $z_i \to z_i$ of coordinates followed by energy minimization. We generate configurations close to the jamming strain γ_j and identify γ_j as follows: We increment strain in steps of $\delta\gamma = 10^{-3}$ until $\frac{e}{N} > e_{\text{thresh}} = 10^{-7}$ at which point we redefine the strain step and threshold energy as $\delta\gamma \to -1 \times \delta\gamma/10$ and $e_{\text{thresh}} \to e_{\text{thresh}}/10$. The system is strained in the reverse direction until $\frac{e}{N} < 10^{-20}$ where updates to e_{thresh} and $\delta\gamma$ are implemented again. This procedure is stopped when $\delta\gamma < 10^{-6}$ and $\frac{e}{N} < 10^{-20}$ and the system is being reverse strained.

Using this procedure we are able to obtain configurations close to the jamming strain, but to study the marginal stability of the shear jamming transition, we need to generate configurations that are *just* shear jammed. Quantitatively this means the configurations have a single self-stress state, or the contact network has one unique force-balance solution [18]. For a given jammed configuration with N_c contacts and N particles which are not rattlers, the number of self-stressed states is given by $N_{ss} = N_c - (N - 1)d$ with periodic boundary conditions [18]. We observe that for large system size configurations obtained using the SJ procedure to obtain shear jammed configurations are not close enough to jamming and have multiple self-stressed states.

To obtain configurations with single self-stressed state we adapt the procedure described for isotropic jamming in Ref. [18] for shear jamming. Starting with a configuration at $d\gamma \equiv (\gamma - \gamma_j) = 10^{-5}$ as determined through the SJ procedure, we iteratively reduce the strain by exploiting the scaling of the potential energy $U \sim (\gamma - \gamma_j)^2$ (which is indeed observed as shown in the Supplemental Material (SM) [36] in addition to further details of this procedure). Using this procedure we generate shear-jammed configurations with a single self-stressed state, whose structure and forces we analyze to
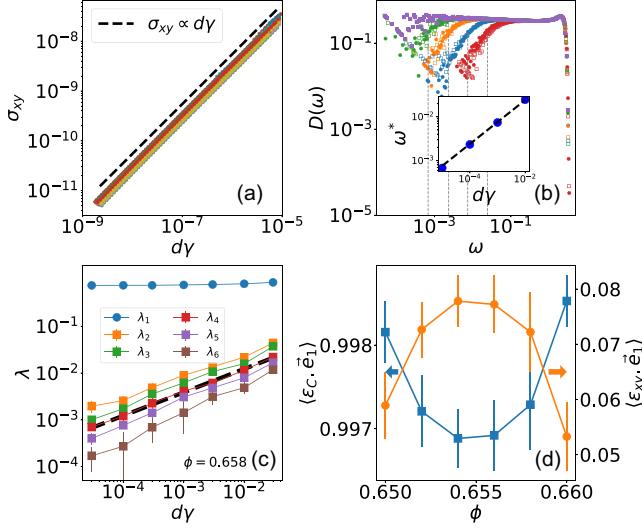
FIG. 2. (a) Stress σ_{xy} vs $d\gamma = \gamma - \gamma_j$ obtained by IP with fit line $\sigma_{xy} \sim d\gamma$. (b) VDOS $D(\omega)$ of configurations at various $d\gamma$'s. The green, orange, blue, and red symbols represent $d\gamma = 10^{-5}$, 10^{-4}, 10^{-3}, and 10^{-2}, respectively. The square and circle symbols represent $\phi = 0.658, 0.656$, respectively. The violet curve is $D(\omega)$ calculated for isotropically jammed configurations with $N_{SS} = 1$. The inset: The crossover frequency ω^* is calculated by choosing the frequency at which $D(\omega)$ becomes approximately half of the plateau value. These values are marked in (b). The spaced line shows the scaling $\omega^* \sim d\gamma^{1/2}$. (c) Eigenvalues of the stiffness matrix λ_i as a function of $d\gamma$ (for $N = 8192$). One eigenvalue is significantly larger than the others and this corresponds to the bulk and shear modulus C_{xyxy}. The dashed line denotes an exponent of $\frac{1}{2}$. $\lambda_i > \lambda_{i+1}$. (d) Inner product of the eigenvector corresponding to the largest eigenvalue $\vec{e}_1$ of the stiffness matrix (for $d\gamma = 10^{-5}$) with compressive (blue squares) and shear (orange circles) strain directions.

study the marginal stability condition. We follow similar procedures for the data regarding the isotropic case with density instead of the strain as the control variable.

The components of the stress tensor are calculated using $\sigma_{\alpha\beta} = \frac{1}{V} \sum_{i<j} f_{ij}^{\alpha} r_{ij}^{\beta}$, where f_{ij}'s are the interparticle forces and the pressure as $P = \frac{1}{3} \text{tr}(\sigma)$. We calculate the density of states $D(\omega)$ which is the distribution of $\omega = \sqrt{\lambda}$ where λ's are the eigenvalues of the Hessian for configurations over a range of strains above the jamming strain. As in the case of isotropic jamming we observe a plateau in $D(\omega)$ for small ω before $D(\omega)$ decreases to zero as $\omega \to 0$. The frequency ω^* at which $D(\omega)$ decreases to half the plateau value is identified as the crossover frequency.

We note that the jammed configurations analyzed contain *rattlers*, particles with less than $d + 1$ contacts. We remove rattlers recursively by identifying them in each iteration from the configurations until no rattlers remain. The percentage of rattler particles is approximately 0.05% for the cases considered. The average contact number as well as distribution of gaps and forces reported are obtained after the rattlers are removed. However, the packing fractions we report are calculated with the total number of particles.

Results. In Fig. 2(a), we show the variation of the shear stress σ_{xy} vs $d\gamma$ for 3D, demonstrating linear behavior $\sigma_{xy} \sim$

$d\gamma$ above the jamming strain. The pressure exhibits the same linear behavior and the excess contact number $\delta z = z - z_c$ varies with the distance from the jamming strain as $\delta z \sim \sqrt{d\gamma}$ with $z_c = 2d$ as observed for isotropic jamming. These results are shown in the SM along with the corresponding results for 2D. In Fig. 2(b), we show the VDOS $D(\omega)$, which exhibits a plateau at low frequencies corresponding to excess modes, which extend towards zero frequency as the jamming strain is approached from above. The frequency at which the crossover to the plateau occurs $\omega^* \sim \delta\phi^{1/2}$ for isotropic jamming [6,8], and we observe the same scaling near the shear jamming transition as shown in Fig. 2(b)(inset). In Fig. 2(c), we show the eigenvalues of the stiffness matrix (details of whose calculation are provided in the SM), investigated in Ref. [26] for shear jamming in frictionless packings. As in Ref. [26], we find a nearly constant largest eigenvalue that is finite at the shear jamming point, and five nearly degenerate (but less so than in Ref,. [26]) eigenvalues which are zero at shear jamming, and whose magnitude grows roughly as $d\gamma^{1/2}$ for larger strains. In Fig. 2(d) we show the overlap of the eigenvector corresponding to the largest eigenvalue with the bulk strain direction and the shear strain direction as a function of density ϕ. Interestingly, the overlap of shear strain with the stiffest eigenvector shows a nonmonotonic behavior. This is correlated with the anisotropy of the configurations at shear jamming, quantified by the fabric anisotropy, which also shows a similar nonmonotonic behavior with changing ϕ as shown in the SM and observed in Ref. [28]. These results taken together demonstrate that the nature of criticality near the shear jamming point is the same as that near the isotropic jamming point.

We now describe the results regarding the forces and the structure of the shear jammed configurations. It is convenient to consider the cumulative probability of forces $G(f) = \int_0^f P(f')df'$. With the gap defined as $h = \frac{r-\sigma}{\sigma}$, the cumulative probability of gaps is $G(h) = \int_0^h P(h')dh'$. For isotropic jamming, the cumulative probability for forces (normalized to the mean value) is described by a power-law $G(f/\langle f \rangle) \sim f^{1+\theta}$ and for gaps $G(h) \sim h^{1-\gamma}$. As shown in Ref. [11] contacts carrying small forces can be mechanically isolated or be strongly coupled with the rest of the system. Opening a mechanically isolated contact will result in only a local rearrangement of the contact network, whereas opening a strongly coupled contact will result in an extended response. Small forces which correspond to localized modes have a distribution characterized by exponent θ_l, and the forces corresponding to extended modes are characterized by exponent θ_e. The inequalities discussed in Ref. [11] in the two cases are as follows:

$$\gamma \geqslant \frac{1}{2 + \theta_e}, \qquad \gamma \geqslant \frac{1 - \theta_l}{2}. \tag{1}$$

If the jammed system is marginally stable and the above inequalities Eq. (1) are saturated (if they become equalities) then the following relation holds:

$$\theta_e \gamma = \theta_l. \tag{2}$$

The force distribution calculated by including all the forces in the system is characterized by exponent $\theta = \min(\theta_l, \theta_e)$. In order to extract θ_l and θ_e, we have to identify contacts
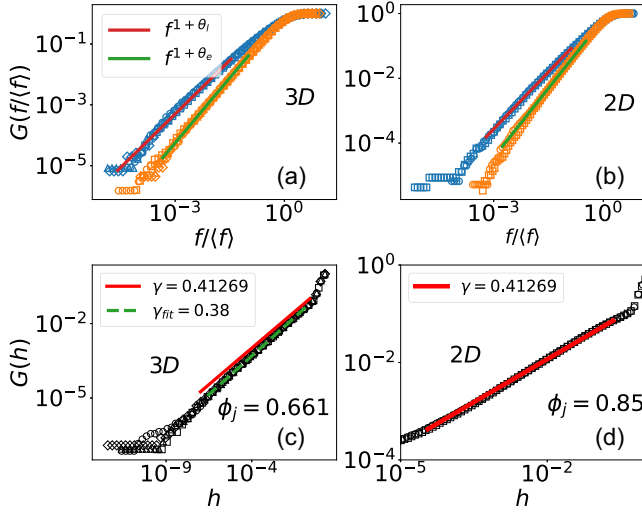
FIG. 3. Interparticle forces and gaps in shear jammed configurations and comparison with isotropically jammed configurations. All configurations analyzed have a single self-stressed state. Symbols $\diamond$, $\bigcirc$, $\square$, and $\triangle$ represent isotropic compression $\phi = 0.660, 0.658, 0.656$, respectively, in 3D and symbols $\bigcirc$, $\square$ represent $\phi = 0.8499, 0.8485$ in 2D. (a) and (b) The cumulative distribution of forces $G(f/\langle f \rangle)$. The blue symbols represent localized forces, and the orange symbols represent the extended forces. Comparison with exponents obtained from mean-field theory is shown. (c) and (d) The cumulative distribution of gaps h. The red line shows the exponent from mean-field theory.

associated with localized and extended modes correctly. Although the mean-field theory of hard-sphere glasses does not contain a prediction for θ_l, based on the predicted values of $\theta_e = 0.423\,11\cdots$ and $\gamma = 0.412\,68\cdots$ and Eq. (2), one has $\theta_l = 0.174\,62$. Charbonneau *et al.* [18] explored how to identify the contacts which carry small mechanically isolated forces. The mechanically isolated contacts are associated with buckler particles which are particles with $d+1$ contacts. As shown in Ref. [18] the force distribution calculated by including only the bucklers $P_l(f)$ exhibits an exponent of $\theta_l = 0.174\,62$. The force exponent calculated by using the distribution of the remaining forces is $P_e(f)$ shows an exponent of $\theta_e = 0.423\,11$. We follow the same procedure to analyze configurations with a single self-stressed state identified by $N_c = (N-1)d + 1$. As opposed to isotropic jamming for the shear jamming transition we need take into account the effect of shear whereas classifying bucklers. However, we observe that for configurations at small strains, classification of bucklers as particles with $d+1$ contacts is sufficient to obtain meaningful results. The cumulative probabilities of forces, separately for bucklers (localized modes) and the rest (extended modes), shown in Figs. 3(a) and 3(b) for 3D and 2D, show that indeed, the predicted values of θ_e and θ_l describe the data extremely well.

In Figs. 3(c) and 3(d) we show the distribution of gaps for 3D and 2D. For 3D, whereas we find the mean-field prediction of $\gamma = 0.412\,68\cdots$ closely describes the data, a value of $\gamma = 0.38$ is a better description of the data. Indeed, results in several works [11,16,28,37], both for isotropic and shear jamming, are consistent with such a smaller exponent, which would correspond to a weak violation of the stability condition. However, the role of finite size effects in the observed departures at very small gaps has recently been investigated [37], emphasizing that finite size effects are much more pronounced for gaps rather than forces. A scaling collapse over several orders of magnitude supports the accuracy of the mean-field exponent for three dimensional packings. Our analysis of finite size effects for shear jamming, shown in the SM, clearly support the same conclusion. On the other hand, the results for 2D, shown in Fig. 3(d) agree very well with the mean-field predictions. Thus, we conclude that the marginal stability conditions [Eq. (1)], which have been shown to be valid for isotropic jamming, *are* indeed also valid for shear jamming.

To summarize, we have numerically analyzed configurations of soft spheres in two and three dimensions accurately generated at the shear jamming point, and above, for densities below the density ϕ_j at which they exhibit isotropic jamming but above the minimum isotropic jamming density ϕ_J. We show that several quantities, such as the pressure P, the excess contact number, and a crossover frequency ω^* in the VDOS $D(\omega)$ exhibit critical scaling that is identical to that at the isotropic jamming point with the shear stress in addition displaying the same scaling as the pressure. We confirm the behavior of the eigenvalues of the stiffness matrix which have been investigated [26] to argue that shear jamming has the same symmetry as isotropic jamming and show that the rotation of the eigenvector of the largest eigenvalue in the shear strain direction is correlated with the anisotropy of the shear jammed structures. We show that the marginal stability condition is met for shear jamming to the same degree as for isotropic jamming with exponents predicted by the mean-field theory of the glass transition and jamming in hard spheres (although our results indicate that better finite size analysis is warranted for the gap distribution). Our results, thus, strongly support the idea that shear jamming displays the same critical behavior and marginal stability as isotropic jamming.

[1] A. J. Liu and S. R. Nagel, Jamming is not just cool any more, Nature (London) **396**, 21 (1998).

[2] C. S. O'Hern, L. E. Silbert, A. J. Liu, and S. R. Nagel, Jamming at zero temperature and zero applied

stress: The epitome of disorder, Phys. Rev. E **68**, 011306 (2003).

[3] M. van Hecke, Jamming of soft particles: geometry, mechanics, scaling and isostaticity, J. Phys.: Condens. Matter **22**, 033101 (2010).

[4] A. J. Liu and S. R. Nagel, The jamming transition and the marginally jammed solid, Annu. Rev. Condens. Matter Phys. **1**, 347 (2010).

[5] P. Chaudhuri, L. Berthier, and S. Sastry, Jamming Transitions in Amorphous Packings of Frictionless Spheres Occur over a Continuous Range of Volume Fractions, Phys. Rev. Lett. **104**, 165701 (2010).

[6] M. Wyart, On the rigidity of amorphous solids, Ann. Phys. (Paris), **30**, 1 (2005)

[7] M. Wyart, L. E. Silbert, S. R. Nagel, and T. A. Witten, Effects of compression on the vibrational modes of marginally jammed solids, Phys. Rev. E **72**, 051306 (2005).

[8] M. Wyart, S. R. Nagel, and T. A. Witten, Geometric origin of excess low-frequency vibrational modes in weakly connected amorphous solids, Europhys. Lett. **72**, 486 (2005).

[9] C. P. Goodrich, A. J. Liu, and J. P. Sethna, Scaling ansatz for the jamming transition, Proc. Natl. Acad. Sci. USA **113**, 9745 (2016).

[10] M. Wyart, Marginal Stability Constrains Force and Pair Distributions at Random Close Packing, Phys. Rev. Lett. **109**, 125502 (2012).

[11] E. Lerner, G. Düring, and M. Wyart, Low-energy non-linear excitations in sphere packings, Soft Matter **9**, 8252 (2013).

[12] G. Combe and J.-N. Roux, Strain versus Stress in a Model Granular Material: A Devil's Staircase, Phys. Rev. Lett. **85**, 3628 (2000).

[13] Y. Jin and H. Yoshino, Exploring the complex free-energy landscape of the simplest glass by rheology, Nat. Commun. **8**, 1 (2017).

[14] P. Charbonneau, J. Kurchan, G. Parisi, P. Urbani, and F. Zamponi, Glass and jamming transitions: From exact results to finite-dimensional descriptions, Annu. Rev. Condens. Matter Phys. **8**, 265 (2017).

[15] G. Parisi, P. Urbani, and F. Zamponi, *Theory of Simple Glasses: Exact Solutions in Infinite Dimensions* (Cambridge University Press, Cambridge, UK, 2020).

[16] P. Charbonneau, E. I. Corwin, G. Parisi, and F. Zamponi, Universal Microstructure and Mechanical Stability of Jammed Packings, Phys. Rev. Lett. **109**, 205501 (2012).

[17] E. DeGiuli, E. Lerner, C. Brito, and M. Wyart, Force distribution affects vibrational properties in hard-sphere glasses, Proc. Natl. Acad. Sci. USA **111**, 17054 (2014).

[18] P. Charbonneau, E. I. Corwin, G. Parisi, and F. Zamponi, Jamming Criticality Revealed by Removing Localized Buckling Excitations, Phys. Rev. Lett. **114**, 125504 (2015).

[19] D. Bi, J. Zhang, B. Chakraborty, and R. P. Behringer, Jamming by shear, Nature (London) **480**, 355 (2011).

[20] J. Ren, J. A. Dijksman, and R. P. Behringer, Reynolds Pressure and Relaxation in a Sheared Granular System, Phys. Rev. Lett. **110**, 018302 (2013).

[21] H. A. Vinutha and S. Sastry, Disentangling the role of structure and friction in shear jamming, Nat. Phys. **12**, 578 (2016).

[22] H. A. Vinutha and S. Sastry, Force networks and jamming in shear-deformed sphere packings, Phys. Rev. E **99**, 012123 (2019).

[23] H. A. Vinutha, K. Ramola, B. Chakraborty, and S. Sastry, Timescale divergence at the shear jamming transition, Granular Matter **22**, 16 (2020).

[24] N. Kumar and S. Luding, Memory of jamming–multiscale models for soft and granular matter, Granular Matter **18**, 58 (2016).

[25] Y. Jin, P. Urbani, F. Zamponi, and H. Yoshino, A stability-reversibility map unifies elasticity, plasticity, yielding, and jamming in hard sphere glasses, Sci. Adv. **4**, eaat6387 (2018).

[26] M. Baity-Jesi, C. P. Goodrich, A. J. Liu, S. R. Nagel, and J. P. Sethna, Emergent SO (3) symmetry of the frictionless shear jamming transition, J. Stat. Phys. **167**, 735 (2017).

[27] V. Babu, D. Pan, Y. Jin, B. Chakraborty, and S. Sastry, Dilatancy, shear jamming, and a generalized jamming phase diagram of frictionless sphere packings, Soft Matter **17**, 3121 (2021).

[28] Y. Jin and H. Yoshino, A jamming plane of sphere packings, Proc. Natl. Acad. Sci. USA **118**, e2021794118 (2021).

[29] A. Peshkov and S. Teitel, Critical scaling of compression-driven jamming of athermal frictionless spheres in suspension, Phys. Rev. E **103**, L040901 (2021).

[30] T. Bertrand, R. P. Behringer, B. Chakraborty, C. S. O'Hern, and M. D. Shattuck, Protocol dependence of the jamming transition, Phys. Rev. E **93**, 012901 (2016).

[31] P. Urbani and F. Zamponi, Shear Yielding and Shear Jamming of Dense Hard Sphere Glasses, Phys. Rev. Lett. **118**, 038001 (2017).

[32] P. Das, H. A. Vinutha, and S. Sastry, Unified phase diagram of reversible–irreversible, jamming, and yielding transitions in cyclically sheared soft-sphere packings, Proc. Natl. Acad. Sci. USA **117**, 10203 (2020).

[33] J. A. Anderson, M. E. Irrgang, and S. C. Glotzer, Scalable metropolis monte carlo for simulation of hard shapes, Comput. Phys. Commun. **204**, 21 (2016).

[34] J. A. Anderson, J. Glaser, and S. C. Glotzer, Hoomd-blue: A python package for high-performance molecular dynamics and hard particle monte carlo simulations, Comput. Mater. Sci. **173**, 109363 (2020).

[35] S. Plimpton, Fast parallel algorithms for short-range molecular dynamics, J. Comput. Phys. **117**, 1 (1995).

[36] See Supplemental Material at http://link.aps.org/supplemental/10.1103/PhysRevE.105.L042901 for the additional information on: (i) details of the iterative procedure (IP), (ii) derivation of the expression for elastic constants, (iii) fabric anisotropy of the shear jammed configuration, (iv) results for pressure and contact number for 2D and 3D, (v) size dependence of the shear jamming line vs density and finite size scaling of the gap distribution, which includes additional Refs. [38,39].

[37] P. Charbonneau, E. I. Corwin, R. C. Dennis, R. Díaz Hernández Rojas, H. Ikeda, G. Parisi, and F. Ricci-Tersenghi, Finite-size effects in the microscopic critical properties of jammed configurations: A comprehensive study of the effects of different types of disorder, Phys. Rev. E **104**, 014102 (2021).

[38] A. Lemaître and C. Maloney, Sum rules for the quasi-static and visco-elastic response of disordered solids at zero temperature, J. Stat. Phys. **123**, 415 (2006).

[39] C. P. Goodrich, S. Dagois-Bohy, B. P. Tighe, M. van Hecke, A. J. Liu, and S. R. Nagel, Jamming in finite systems: Stability, anisotropy, fluctuations, and scaling, Phys. Rev. E **90**, 022138 (2014).